A Hybrid Arithmetic Smell Agent Optimization Algorithm for Stability Control of Micro-Grid Systems

Ndukwe Okpo Kalu
Department of Electrical and Electronics Engineering, Nile University of Nigeria, Nigeria
obinnandukwe60@yahoo.com

Oghenewvogaga Oghorada
Department of Electrical and Electronics Engineering, Nile University of Nigeria, Nigeria
oghenewvogaga.oghorada@nileuniversity.edu.ng

Omotayo Oshiga
Department of Electrical and Electronics Engineering, Nile University of Nigeria, Nigeria
ooshiga@nileuniversity.edu.ng

Jibril Abdullahi Bala
Department of Mechatronics Engineering, Federal University of Technology, Minna, Nigeria
jibril.bala@futminna.edu.ng (corresponding author)

Received: 27 May 2025 | Revised: 21 June 2025 and 9 July 2025 | Accepted: 11 July 2025

 DOI: https://doi.org/10.48084/etasr.12400

ABSTRACT

Microgrid systems play a vital role in meeting local energy demands, particularly in the presence of unpredictable load variations. However, maintaining system stability under such conditions remains a key challenge. Despite several works implementing optimized control strategies, they are limited in their ability to offer robust solutions for addressing the complex interplay of power quality, stability, efficiency, and load variations in microgrids. This study addresses that limitation by presenting a hybrid Arithmetic Smell Agent Optimization (ASAO) algorithm, designed to optimize microgrid control performance by effectively tuning Proportional–Integral–Derivative (PID) parameters. A Simulink model was developed, incorporating solar Photovoltaic (PV) generation, battery energy storage, and grid interconnection, to simulate microgrid behavior. The control system adopted a two-level hierarchy, with a primary controller for rapid disturbance correction and a secondary controller for long-term stability. The primary and secondary controllers demonstrated rapid stabilization, with rise times of 4 ms and 50 ms, and settling times of 4.1 ms and 75 ms, respectively. This work provides a reliable foundation for the design of intelligent control systems in modern microgrids, offering scalable and efficient solutions for sustainable power delivery.

Keywords-arithmetic optimization algorithm; load variations; microgrid control; Proportional–Integral–Derivative (PID) controller; Arithmetic Smell Agent Optimization (ASAO)

I. INTRODUCTION

A microgrid is a geographically regulated and coordinated network of dispersed power sources, loads, and distribution network resources that can operate in an islanded or grid-connected manner [1]. One of the primary responsibilities of a microgrid is to ensure optimization and stability control. Optimization supports efficient energy dispatch for maximum economic benefit, while control ensures frequency and voltage regulation to maintain system stability and power quality [2]. Among the various performance indicators, power flow stability, particularly via frequency regulation and power quality, serves as a critical metric for assessing overall system reliability in microgrids [3].

However, controlling these parameters has become increasingly challenging due to factors such as nonlinear load dynamics, reduced inertia, operational uncertainties, and the intermittent nature of renewable energy sources [4]. Load variations, in particular, introduce disturbances that disrupt frequency stability and power flow, potentially degrading

power quality, posing operational safety risks, and damaging connected infrastructure [5].

Recent advancements in Load Frequency Control (LFC) have addressed these challenges through diverse control strategies, ranging from conventional Proportional–Integral–Derivative (PID) controllers to Model Predictive Control (MPC) and metaheuristic optimization techniques. Despite their promise, robust frequency regulation in multi-source microgrids remains challenging due to the inherent unpredictability of renewables and the dynamic nature of load profiles [6].

Several studies have proposed hierarchical and decentralized control schemes to enhance system resilience. For instance, authors in [7] introduced a supervisory predictive LFC mechanism for a four-area power system, demonstrating improved performance over decentralized PI control. However, MPC's computational overhead remains a significant drawback, requiring more efficient yet effective control approaches. Similarly, authors in [8] proposed a modified load disturbance rejection technique for isolated microgrids, which outperformed traditional PID controllers but suffered from high peak deviations in worst-case scenarios.

Among optimization strategies, metaheuristic algorithms have been widely used to tune controller parameters. For example, authors in [9] and [10] employed Genetic Algorithms (GA) and Quasi-Oppositional Harmony Search (QOHS) to optimize droop and PID parameters, respectively. While such methods have improved frequency stability, they often encounter slow convergence rates or premature convergence to suboptimal solutions. Hybrid algorithms such as the Whale-Pattern Search (WPS) [11] and Improved Salp Swarm Algorithm (ISSA) [12] have addressed some of these limitations but still face challenges in achieving rapid settling times and minimizing overshoot under dynamic disturbances.

Intelligent control strategies have also been explored. For example, authors in [13] proposed a fuzzy logic-based energy management system for hybrid microgrids to ensure an uninterrupted power supply. In a similar vein, authors in [14] introduced an adaptive fuzzy PID controller optimized using an Improved Sine-Cosine Algorithm (ISCA), demonstrating enhanced stability. Nonetheless, these methods often demand extensive parameter tuning and struggle with real-time adaptation to unpredictable renewable output.

Despite these advancements, two significant gaps remain in the literature:

- Suboptimal PID parameter tuning using traditional or inefficient optimization techniques leads to delayed frequency restoration and unacceptable overshoots [15, 16].
- Single-level control architectures are inadequate for modern microgrids, which involve complex, multi-source, and highly dynamic operating conditions [16, 17–19].

While metaheuristic techniques such as PSO and GA have shown some effectiveness [12, 20], they often suffer from premature convergence and lack the flexibility to escape local optima. On the other hand, although hierarchical control schemes offer superior coordination [7], their implementation is often resource-intensive, raising concerns about computational feasibility and system complexity.

This study addresses the aforementioned challenges by proposing a hybrid Arithmetic Smell Agent Optimization (ASAO) algorithm, specifically tailored for tuning PID parameters in microgrid control applications. The hybrid ASAO combines the robust global search capabilities of the Smell Agent Optimization (SAO) algorithm with the efficient local search refinement of the Arithmetic Optimization Algorithm (AOA). This synergistic approach enables effective navigation of complex, nonlinear search spaces, ensuring rapid convergence without compromising global optimality. The core contributions of this study are as follows:

- Design and development of a dual-level PID-based stability controller for microgrid systems.
- Formulation of the ASAO hybrid optimization algorithm for enhanced controller tuning.
- Comprehensive performance comparison of ASAO against standalone SAO and AOA algorithms under varying load conditions.
- Simulation of a solar Photovoltaic (PV)–battery–grid-connected microgrid using MATLAB/Simulink to validate controller performance.

II. RESEARCH METHODOLOGY

A. Microgrid Model

The microgrid model employed in this study, adapted from [21] and shown in Figure 1, highlights the fundamental components necessary for basic operational functionality. The model comprises three discrete load units, a solar PV generation system, a Battery Energy Storage System (BESS), and an interface for grid interconnection. These elements collectively represent the essential infrastructure for modern microgrid operation. Each plays a critical role in maintaining system power balance and operational stability. Both the solar PV and BESS are modeled as Direct Current (DC) power sources, which are converted to single-phase Alternating Current (AC) to ensure compatibility with load and grid requirements.

A key assumption of the control strategy is the semi-autonomous capability of the microgrid, whereby the combined output from the solar and battery units is sufficient to satisfy local demand under normal operating conditions. This design facilitates reduced grid dependency, enhanced resilience, and supports sustainable energy integration within the system.

B. Two-Level Controller

The design and formulation of the two-level hierarchical control scheme for LFC in microgrids are presented in Figure 2. A key distinguishing feature of this control architecture is the selection of root mean square current I_{RMS} as the control variable, in contrast to conventional LFC approaches that typically rely on power-based signals. The choice of I_{RMS} is motivated by its ability to offer faster and more precise real-time indications of load variations compared to frequency

deviation alone. This leads to an enhanced dynamic response, superior integration with current-controlled power electronics, and greater system stability in modern hybrid power systems. To ensure robust and precise frequency regulation, PID controllers are integrated at both the primary and secondary control levels.

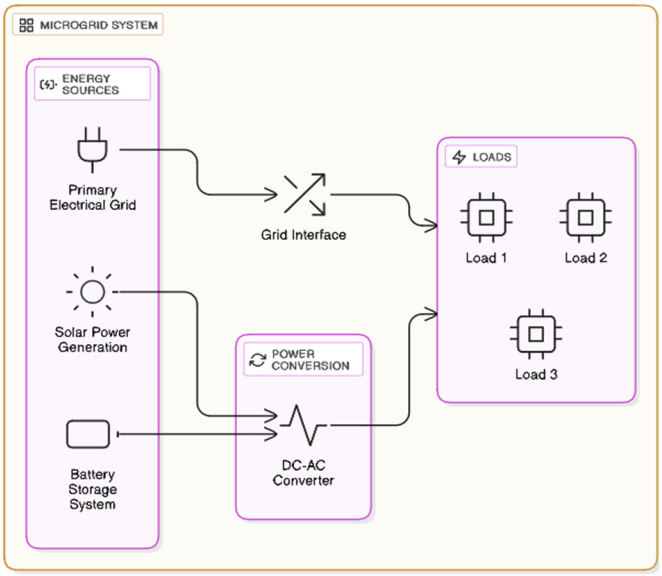

Fig. 1. Representation of microgrid model.

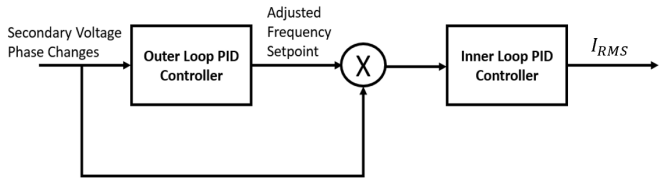

Fig. 2. Two-level stability controller architecture.

The primary control mechanism is responsible for rapidly responding to frequency fluctuations that arise within the microgrid. Its primary function is to detect anomalies in system frequency and compute the necessary I_{RMS} adjustments to restore stability. This fast-reacting control layer ensures prompt correction of transient disturbances, making it integral to short-term frequency regulation.

The control input to the primary controller is the frequency deviation Δf, defined as the difference between the observed system frequency and the nominal reference frequency. The PID controller processes this deviation and generates a real-time control signal to regulate current output and thus stabilize frequency. Mathematically, the PID controller can be formulated from the standard PID equation [22] as:

$$I_{RMS} = K_p \Delta f + K_i \int \Delta f dt + K_d \frac{d(\Delta f)}{dt} \quad (1)$$

where K_p, K_i, and K_d are the proportional, integral, and derivative gains, respectively.

The secondary controller complements the primary loop by addressing long-term and persistent frequency deviations that accumulate over time. Its purpose is to ensure zero steady-state error and long-term system accuracy. This is achieved by monitoring the Area Control Error (ACE), which represents the cumulative frequency discrepancy and acts as a key performance indicator in power system control. Mathematically, the secondary PID controller can be formulated based on [23] as:

$$\Delta f_{adjusted} = K_{p2} ACE + K_{i2} \int ACE\, dt + K_{d2} \frac{d(ACE)}{dt} \quad (2)$$

where K_{p2}, K_{i2}, and K_{d2} are the proportional, integral, and derivative gains of the secondary controller, and ACE signifies the integrated value of the frequency deviation over time. The output, $\Delta f_{adjusted}$, provides a bias to the primary controller, influencing its effective setpoint and subsequently its I_{RMS} command.

C. Hybrid Arithmetic Smell Agent Optimization (ASAO)

To enhance the performance of AOA, we propose a hybrid framework wherein the SAO algorithm is employed to dynamically tune AOA's critical parameters, Alpha (α) and Mu (μ). This adaptive parameter optimization ensures a superior trade-off between exploration and exploitation, thereby improving convergence speed and solution quality. The proposed hybrid ASAO algorithm is presented below:

```
Algorithm 1: Hybrid ASAO Algorithm
Input: Population size N, Max iterations
M(iter), Lower bound LB, Upper bound UB,
Dimension Dim, Objective function F(obj)
Output: Best fitness value Hybrid_Best_FF,
Best solution Hybrid_Best_P
Initialize SAO Parameters
Set number of smell agents: SAO_Molecules
= 10
Set SAO max iterations: SAO_Max_Iter = 20
Define bounds for parameters: α ∈ [1, 10],
μ ∈ [0.1, 1]
Define SAO objective function: f(SAO) ←
AOA_Cost(α, μ, N, M(iter), LB, UB, Dim, F(obj))
Run SAO to optimize α and μ
Obtain optimal values: Optimal_Alpha,
Optimal_Mu
Run AOA with Optimized Parameters:
Initialize population X randomly within LB
and UB
Compute fitness for initial solutions
Set best fitness Best_FF = ∞, best
position Best_P
For C(iter) = 1 to M(iter) do
    Compute material properties MOP, MOA
    for each solution Xi do
        for each dimension j do
            Update position using AOA
update rules with α, μ
            Apply boundary constraints
 end for
```

```
 Evaluate new fitness
  if new fitness is better then
      Update best solution
end for
Update convergence curve
end for
return Hybrid_Best_FF, Hybrid_Best_P
```

The ASAO algorithm was configured with a maximum of 1000 iterations and 20 search solutions, with the stopping criterion set as the convergence of the solution curve. The lower and upper bounds of the μ parameter were set between 0.1 and 1, respectively, while for the α parameter, they were set between 1 and 10. The parameter tuning process begins with an initialization phase, where SAO generates a population of candidate values for α and μ.

The SAO process then iteratively applies sniffing, trailing, and random movement operations to explore the solution space. Inferior candidates are progressively replaced by more promising ones based on their fitness values, as determined by the AOA cost function. This selection pressure enables the swarm to converge toward optimal parameter settings. Upon reaching the stopping criterion, either convergence of the fitness curve or the maximum number of iterations, the best-performing values of α and μ are selected as the final configuration. Then, the AOA is executed to address the primary optimization problem. AOA is designed based on fundamental arithmetic principles and operates through a structured sequence of phases, ensuring an effective balance between exploration and exploitation to achieve high-quality solutions.

D. Performance Evaluation of ASAO Using Benchmark Functions

Benchmark functions are indispensable for assessing the effectiveness and robustness of optimization algorithms. They are specifically designed to evaluate various aspects of algorithmic performance, including the ability to avoid local optima (global search/exploration), the capacity to fine-tune solutions (local search/exploitation), convergence characteristics (speed and smoothness), and robustness across diverse problem landscapes.

In this study, the selected benchmark functions encompass unimodal, multimodal, and composite types, with varying levels of dimensionality and complexity. This diversity provides a comprehensive basis for evaluating the ASAO algorithm's capability to address a wide range of optimization challenges, closely resembling those encountered in real-world engineering applications, such as microgrid stability control. Table I summarizes the benchmark functions used, as presented in [24].

TABLE I. SUMMARY OF BENCHMARK FUNCTIONS

Function	**F(x)**	**Function Type**	**F(x) at Global Minimum**
Adjiman Function	$\cos(x_1)\sin(x_2) - \frac{x_1}{x_2^2+1}$	Multimodal	-2.02181
Beale Function	$(1.5 - x_1 + x_1x_2)^2 + (2.25 - x_1 + x_1x_2^2)^2 + (2.625 - x_1 + x_1x_2^3)^2$	Unimodal	0
Bird	$\sin(x_1)e^{(1-\cos(x_2))^2} + \cos(x_2)e^{(1-\cos(x_1))^2} + (x_1 - x_2)^2$	Multimodal	-106.764537
Bohachevsky 1 Function	$x_1^2 + 2x_2^2 - 0.3\cos(3\pi x_1) - 0.4\cos(4\pi x_2) + 0.7$	Multimodal	0
Booth Function	$(x_1 + 2x_2 - 7)^2 + (2x_1 + x_2 - 5)^2$	Unimodal	0
Branin RCOS Function	$\left(x_2 - \frac{5.1x_1^2}{4\pi^2} + \frac{5x_1}{\pi} - 6\right)^2 + 10\left(1 - \frac{1}{8\pi}\right)\cos x_1 + 10$	Multimodal	0.3978873
Branin RCOS 2 Function	$\left(x_2 - \frac{5.1x_1^2}{4\pi^2} + \frac{5x_1}{\pi} - 6\right)^2 + 10\left(1 - \frac{1}{8\pi}\right)\cos x_1 \cos x_2 \ln(x_1^2 + x_2^2 + 1) + 10$	Multimodal	5.559037
Brent Function	$(x_1 + 10)^2 + (x_2 + 10)^2 + e^{-x_1^2 - x_2^2}$	Unimodal	0
Bukin 2 Function	$100(x_2 - 0.01x_1^2 + 1) + 0.01(x_1 + 10)^2$	Multimodal	0
Camel Function (Six Hump)	$\left(4 - 2.1x_1^2 + \frac{x_1^4}{3}\right)x_1^2 + x_1x_2 + (4x_2^2 - 4)x_2^2$	Multimodal	−1.0316
Chichinadze	$x_1^2 - 12x_1 + 11 + 10\cos\left(\frac{\pi x_1}{2}\right) + 8\sin(5\pi x_1/2) - (1/5)^{0.5}\exp(-0.5(x_2 - 0.5)^2)$	Multimodal	−43.3159
Deckkers-Aarts Function	$10^5x_1^2 + x_2^2 - (x_1^2 + x_2^2)^2 + 10^{-5}(x_1^2 + x_2^2)^4$	Multimodal	-247770
Easom Function	$-\cos(x_1)\cos(x_2)\exp[-(x_1 - \pi)^2 - (x_1 - \pi)^2 - (x_2 - \pi)^2]$	Multimodal	-1
Matyas Function	$0.26(x_1^2 + x_2^2) - 0.48x_1x_2$	Unimodal	0
McCormick Function	$\sin(x_1 + x_2) + (x_1 - x_2)^2 - (3/2)x_1 + (5/2)x_2 + 1$	Multimodal	-1.9133
Quadratic Function	$-3803.84 - 138.08x_1 - 232.92x_2 + 128.08x_1^2 + 203.64x_2^2 + 182.25x_1x_2$	Unimodal	−3873.7243
Schaffer Function	$\sum_{i=1}^{D} 0.5 + \frac{\sin^2\sqrt{x_i^2 + x_{i+1}^2} - 0.5}{[1+0.001(x_i^2 + x_{(i+1)}^2)]^2}$	Unimodal	0
Styblinski-Tang Function	$\frac{1}{2}\sum_{i=1}^{n}(x_i^4 - 16x_i^2 + 5x_i)$	Multimodal	−78.332
Box- Betts	$\sum_{i=0}^{D-1} g(x_i)^2$	Multimodal	0
Colville Function	$100(x_1 - x_2^2)^2 + (1 - x_1)^2 + 90(x_4 - x_3^2)^2 + (1 - x_3)^2 + 10.1((x_2 - 1)^2 + (x_4 - 1)^2) + 19.8(x_2 - 1)(x_4 - 1)$	Multimodal	0
Csendes Function	$\sum_{i=1}^{D} x_i^6\left(2 + \sin\frac{1}{x_i}\right)$	Multimodal	0

III. RESULTS AND DISCUSSION

A. Performance of Hybrid ASAO

The hybrid ASAO algorithm was implemented on the Simulink model and evaluated based on its convergence behavior when applied to selected benchmark test functions. To assess, preliminarily, the effectiveness of ASAO in handling different optimization challenges, two test functions were selected:

- The Adjiman function, a multimodal function with multiple local minima, requiring strong exploration capabilities to avoid premature convergence.
- The Beale function, a unimodal function with a single global minimum, testing the algorithm's ability to efficiently perform local exploitation and fine-tune solutions.

The performance of ASAO on these functions was analysed by plotting the convergence curves, which illustrate the reduction in the objective function value as the algorithm progresses. Figure 3 shows the convergence plot of the Adjiman test function, and Figure 4 of the Beale function.

As shown in Figure 3, the convergence curve for ASAO demonstrates how the algorithm navigates a highly rugged search space. The objective function value drops sharply after the 800th iteration, reflecting ASAO's active exploration of different regions and its ability to avoid premature convergence to local minima. As the iterations progress, the convergence rate gradually slows, marking the transition from broad exploration to fine-grained local search. The final stabilization of the curve confirms ASAO's effectiveness in handling multimodal landscapes, making it well-suited for optimization problems involving multiple decision variables and constraints.

In contrast, the convergence behavior for the Beale test function, shown in Figure 4, highlights ASAO's adaptability. The convergence curve exhibits a steep descent after the 900th iteration, indicating that the algorithm quickly identifies the optimal region. Here, ASAO swiftly transitions to fine-tuning within a narrow range, achieving stable convergence in fewer iterations. The final plateau of the curve demonstrates that ASAO minimizes the function value with high precision and minimal computational overhead.

A comprehensive overview of the optimization performance for 22 benchmark functions is presented in Table II. This table consolidates the best results obtained by the AOA, SAO algorithm, and the proposed ASAO algorithm across a diverse set of test functions. The performance metrics considered for comparison include the best solution vector x discovered by each algorithm, and the corresponding objective function value f(x).

From the comparative results, ASAO either matched or surpassed the performance of AOA and SAO on nearly all the benchmark functions in terms of the objective function value. This trend was especially evident in complex, multimodal functions (e.g., Bird, Deckers-Aarts, Michalewicz) where the landscape includes numerous local minima that typically trap conventional algorithms. These functions are well-known for their deceptive fitness landscapes and require robust exploration strategies to avoid premature convergence.

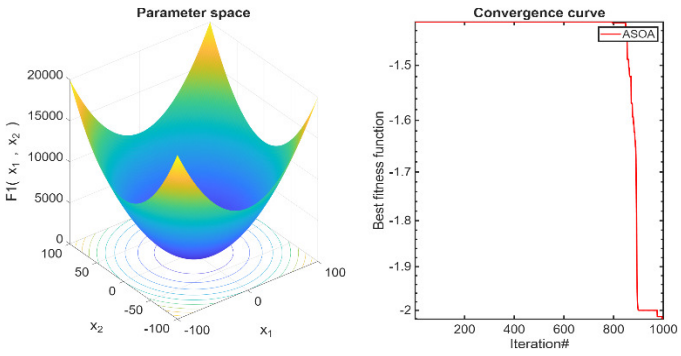

Fig. 3. Convergence curve for the Adjiman test function.

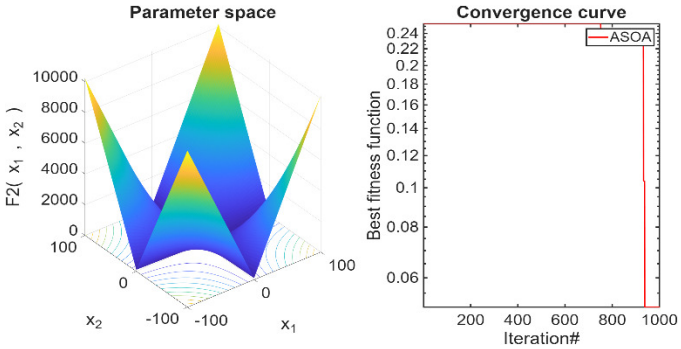

Fig. 4. Convergence curve for the Beale test function.

TABLE II. SUMMARY OF OPTIMIZATION RESULTS – AOA VS SAO VS ASAO

Function	AOA	SAO	ASAO
	f(x)	f(x)	f(x)
Adjiman	-2.0218	-1.9994	-2.0218
Beale	0.9430	1.0527e-05	0.0487
Bird	-98.8761	-1.0678e+02	-89.3907
Bohachevsky 1	0	-1.0678e+02	0
Booth	0.52722	0.3978	0.64871
Branin RCOS	0.4345	0.3978	0.78094
Branin RCOS 2	-0.27647	-0.2777	-0.10352
Brent	1.3839e-87	5.1588e-46	1.3839e-87
Bukin 2	5.0975	5.1218	5.0975
Camel (Six Hump)	-1.0316	-1.0316	-0.1336
Chichinadze	-28.525	-42.4971	-42.4649
Deckkers-Aarts	-24776.5183	-2.4755e+04	-24346.5754
Easom	-1	-0.9999	-0.96371
Matyas	0	9.62593e-09	0
McCormick	-1.0948	-1.9132	-1.6135
Michalewicz	-1.9956	-1.9999	-1.9546
Quadratic	-3873.7241	-3.87377e+03	-3871.8699
Schaffer	0	1.0519e-12	0
Styblinski-Tang	-64.8395	-78.3321	-78.1693
Box- Betts	125.8576	1.2585e+02	125.8576
Colville	10.0887	0	0
Csendes	0	1.8174e-15	0

B. Performance of Optimized Two-level Control System

The Simulink model served as a virtual testbed for evaluating the proposed control strategy under varying

conditions, including unscheduled load variations, power fluctuations, and fault scenarios.

The inner and outer loop control efforts derived from the unoptimized PID controllers are presented in Figures 5 and 6, respectively. Both controllers exhibit a linear increase in control effort, reaching a peak value of approximately 9,000,000. Although this magnitude may appear excessive, it reflects the initial tuning state of the controllers, which have not yet undergone optimization. Such behavior is typical in control systems where parameter settings are suboptimal, resulting in persistent corrective effort to manage deviations. The system expends unnecessary energy and may risk overshoot or prolonged settling times. The controller responses are illustrated in Figures 7 and 8.

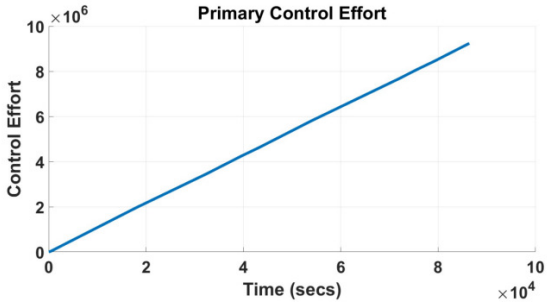

Fig. 5. Primary control effort.

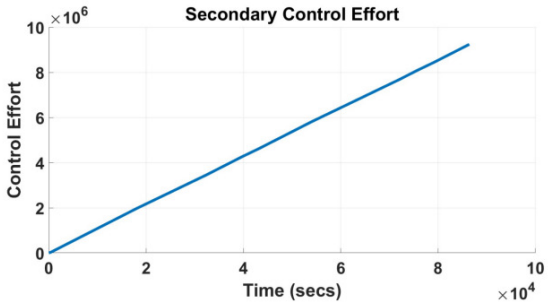

Fig. 6. Secondary control effort.

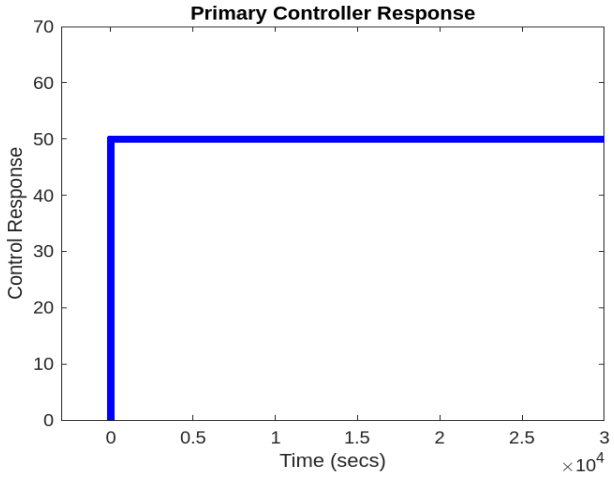

Fig. 7. Output response of the primary controller.

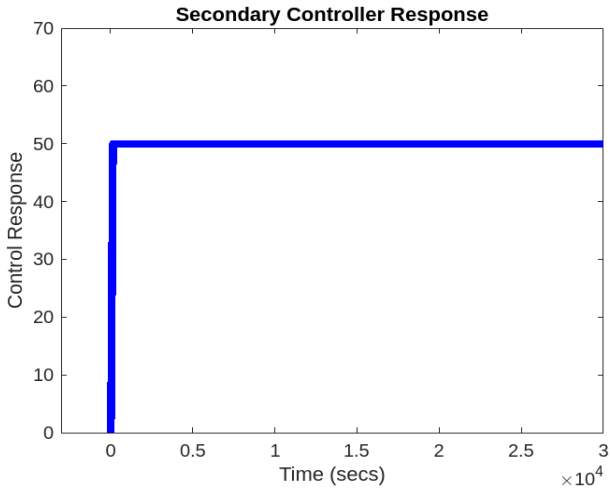

Fig. 8. Output response of the secondary controller.

The primary controller demonstrates good transient response, rapidly stabilizing the system following an initial disturbance. Notably, the controller achieves a rise time of approximately 4 milliseconds, with the response increasing sharply from 0 to 1.4804 at 0.0001 s, then to 4.1356 at 0.00028 s, and finally reaching 49.3187 at 0.0040 s. The settling time is equally impressive, with the output stabilizing at 50.0000 at 0.0041 s, indicating the controller's ability to effectively dampen transient effects and maintain system stability without oscillations or further deviations.

The secondary controller exhibits a rise time of 50 ms and settling time of 75 ms, gradually increasing from 0 to a steady-state of 50.0. Its smooth convergence validates its role as a long-term stabilization mechanism, refining residual frequency deviations and ensuring sustained system accuracy.

IV. CONCLUSION

This study proposed a novel dual-level stability control framework for microgrid systems, underpinned by a hybrid Arithmetic Smell Agent Optimization (ASAO) algorithm. By integrating the global exploration capabilities of the Smell Agent Optimization (SAO) algorithm with the local refinement strength of the Arithmetic Optimization Algorithm (AOA), the ASAO approach effectively addresses the limitations of both conventional single-level controllers and computationally intensive hierarchical strategies in achieving robust and efficient Load Frequency Control (LFC).

The ASAO algorithm was specifically designed to optimize the parameters of Proportional–Integral–Derivative (PID) controllers, ensuring rapid dynamic response and long-term system stability under unscheduled load variations and other disturbances. Through comprehensive benchmark function evaluations, ASAO consistently outperformed or matched its standalone counterparts in terms of solution quality, convergence speed, and computational efficiency. These capabilities were further validated in a Simulink-based microgrid environment, where the ASAO-optimized control system achieved fast stabilization, with rise times of 4 ms (primary controller) and 50 ms (secondary controller), and settling times of 4.1 ms and 75 ms, respectively.

The dynamic simulation results confirmed the resilience and scalability of the proposed ASAO-driven control framework, particularly in managing frequency deviations and maintaining power quality in decentralized microgrid operations. By demonstrating the viability of hybrid metaheuristic techniques in complex control scenarios, this work highlights the potential of ASAO to significantly advance the development of intelligent, adaptive control architectures in future energy systems.

Future work will focus on extending this research through experimental validation, including Hardware-in-the-Loop (HIL) testing, and exploring integration with variable renewable energy sources, to further enhance the adaptability and real-world applicability of the proposed framework.

REFERENCES

[1] A. Bracale, P. Caramia, G. Carpinelli, E. Mancini, and F. Mottola, "Optimal control strategy of a DC micro grid," *International Journal of Electrical Power & Energy Systems*, vol. 67, pp. 25–38, May 2015, https://doi.org/10.1016/j.ijepes.2014.11.003.

[2] D. Yu, H. Zhu, W. Han, and D. Holburn, "Dynamic multi agent-based management and load frequency control of PV/Fuel cell/ wind turbine/ CHP in autonomous microgrid system," *Energy*, vol. 173, pp. 554–568, Apr. 2019, https://doi.org/10.1016/j.energy.2019.02.094.

[3] D. Cao *et al.*, "Reinforcement Learning and Its Applications in Modern Power and Energy Systems: A Review," *Journal of Modern Power Systems and Clean Energy*, vol. 8, no. 6, pp. 1029–1042, 2020, https://doi.org/10.35833/MPCE.2020.000552.

[4] F. Garcia-Torres, A. Zafra-Cabeza, C. Silva, S. Grieu, T. Darure, and A. Estanqueiro, "Model Predictive Control for Microgrid Functionalities: Review and Future Challenges," Energies, vol. 14, no. 5, Feb. 2021, Art. no. 1296, https://doi.org/10.3390/en14051296.

[5] M. F. Roslan, M. A. Hannan, P. J. Ker, and M. N. Uddin, "Microgrid control methods toward achieving sustainable energy management," Applied Energy, vol. 240, pp. 583–607, Apr. 2019, https://doi.org/10.1016/j.apenergy.2019.02.070.

[6] S. A. Shezan *et al.*, "Evaluation of Different Optimization Techniques and Control Strategies of Hybrid Microgrid: A Review," *Energies*, vol. 16, no. 4, Feb. 2023, Art. no. 1792, https://doi.org/10.3390/en16041792.

[7] M. Shiroei and A. M. Ranjbar, "Supervisory predictive control of power system load frequency control," *International Journal of Electrical Power & Energy Systems*, vol. 61, pp. 70–80, Oct. 2014, https://doi.org/10.1016/j.ijepes.2014.03.020.

[8] B. Kumar and S. Bhongade, "Load Disturbance Rejection based PID controller for frequency regulation of a microgrid," in *2016 Biennial International Conference on Power and Energy Systems: Towards Sustainable Energy (PESTSE)*, Bangalore, Jan. 2016, pp. 1–6, https://doi.org/10.1109/PESTSE.2016.7516459.

[9] R. Rahmani and A. Fakharian, "New Control Method of Islanded Microgrid System: A GA & ICA based optimization approach," *The Modares Journal of Electrical Engineering*, vol. 12, no. 4, 2013.

[10] G. Shankar and V. Mukherjee, "Load frequency control of an autonomous hybrid power system by quasi-oppositional harmony search algorithm," *International Journal of Electrical Power & Energy Systems*, vol. 78, pp. 715–734, Jun. 2016, https://doi.org/10.1016/j.ijepes.2015.11.091.

[11] R. K. Khadanga, S. Padhy, S. Panda, and A. Kumar, "Design and analysis of multi-stage PID controller for frequency control in an islanded micro-grid using a novel hybrid whale optimization-pattern search algorithm," *International Journal of Numerical Modelling: Electronic Networks, Devices and Fields*, vol. 31, no. 5, Sep. 2018, Art. no. e2349, https://doi.org/10.1002/jnm.2349.

[12] P. C. Sahu, S. Mishra, R. C. Prusty, and S. Panda, "Improved-salp swarm optimized type-II fuzzy controller in load frequency control of multi area islanded AC microgrid," *Sustainable Energy, Grids and Networks*, vol. 16, pp. 380–392, Dec. 2018, https://doi.org/10.1016/j.segan.2018.10.003.

[13] Z. Roumila, D. Rekioua, and T. Rekioua, "Energy management based fuzzy logic controller of hybrid system wind/photovoltaic/diesel with storage battery," *International Journal of Hydrogen Energy*, vol. 42, no. 30, pp. 19525–19535, Jul. 2017, https://doi.org/10.1016/j.ijhydene.2017.06.006.

[14] K. S. Rajesh and S. S. Dash, "Load frequency control of autonomous power system using adaptive fuzzy based PID controller optimized on improved sine cosine algorithm," *Journal of Ambient Intelligence and Humanized Computing*, vol. 10, no. 6, pp. 2361–2373, Jun. 2019, https://doi.org/10.1007/s12652-018-0834-z.

[15] R. Alayi, F. Zishan, S. R. Seyednouri, R. Kumar, M. H. Ahmadi, and M. Sharifpur, "Optimal Load Frequency Control of Island Microgrids via a PID Controller in the Presence of Wind Turbine and PV," *Sustainability*, vol. 13, no. 19, Sep. 2021, Art. no. 10728, https://doi.org/10.3390/su131910728.

[16] I. Abdulwahab, S. A. Faskari, T. A. Belgore, and T. A. Babaita, "An Improved Hybrid Micro-Grid Load Frequency Control Scheme for an Autonomous System," *FUOYE Journal of Engineering and Technology*, vol. 6, no. 4, Dec. 2021, https://doi.org/10.46792/fuoyejet.v6i4.698.

[17] L. Carrette, K. A. Friedrich, and U. Stimming, "Fuel Cells - Fundamentals and Applications," *Fuel Cells*, vol. 1, no. 1, pp. 5–39, May 2001, https://doi.org/10.1002/1615-6854(200105)1:1<5::AID-FUCE5>3.0.CO;2-G.

[18] A. J. Veronica, N. S. Kumar, and F. Gonzalez-Longatt, "Design of Load Frequency Control for a Microgrid Using D-partition Method," *International Journal of Emerging Electric Power Systems*, vol. 21, no. 1, Feb. 2020, https://doi.org/10.1515/ijeeps-2019-0175.

[19] N. A. Luu and T. L. Nguyen, "Secondary Control for Cyber-Physical Interconnected Microgrid Systems," *Engineering, Technology & Applied Science Research*, vol. 15, no. 2, pp. 21944–21950, Apr. 2025, https://doi.org/10.48084/etasr.10333.

[20] B. Kumar, S. Adhikari, S. Datta, and N. Sinha, "Real Time Simulation for Load Frequency Control of Multisource Microgrid System Using Grey Wolf Optimization Based Modified Bias Coefficient Diagram Method (GWO-MBCDM) Controller," *Journal of Electrical Engineering & Technology*, vol. 16, no. 1, pp. 205–221, Jan. 2021, https://doi.org/10.1007/s42835-020-00596-2.

[21] MathWorks, "Simplified Model of a Small Scale Micro-Grid," MathWorks Documentation, [Online]. Available: https://www.mathworks.com/help/sps/ug/simplified-model-of-a-small-scale-micro-grid.html.

[22] K. Ogata, *Modern control engineering*, 5th ed. Upper Saddle River, NJ, USA: Prentice Hall, 2010.

[23] R. Singh *et al.*, "Design of 2 DOF PID Controller for Load Frequency Control of Two Area Power System using Mfo Algorithm," *International Journal of Engineering and Advanced Technology*, vol. 9, no. 3, pp. 158–161, Feb. 2020, https://doi.org/10.35940/ijeat.C5009.029320.

[24] M. Jamil and X. S. Yang, "A literature survey of benchmark functions for global optimisation problems," *International Journal of Mathematical Modelling and Numerical Optimisation*, vol. 4, no. 2, 2013, Art. no. 150, https://doi.org/10.1504/IJMMNO.2013.055204.